

STRENGTH OF A C-SPHERE FLEXURE SPECIMEN¹

A. A. Wereszczak, W. Wang,[#] O. M. Jadaan,* T. P. Kirkland, M. J. Lance, and H. -T. Lin
Ceramic Science and Technology
Oak Ridge National Laboratory
Oak Ridge, TN 37831

[#] Bournemouth University
Dorset, UK BH12 5BB

* University of Wisconsin - Platteville
Platteville, WI 53818

ABSTRACT

A “C-Sphere” flexure strength specimen geometry was conceived and developed to measure a relevant strength of bearing-grade Si_3N_4 balls and to relate that to surface-located strength-limiting flaws and to ultimately link those flaw populations to rolling contact fatigue performance. A slot was machined into the balls to a set depth to produce the C-sphere geometry. C-sphere specimens were then diametrically compressed to produce a monotonically increasing flexure or hoop tensile stress at their surface that caused their fracture. The strength was determined using the combination of failure load, C-sphere geometry, and FEA, and the stress field was used to determine C-sphere effective areas and effective volumes as a function of Weibull modulus. A description of the specimen and the aforementioned analysis are provided and a comparison of C-sphere flexure strength distributions of two bearing grade Si_3N_4 materials (NBD200 and SN101C) is given.

INTRODUCTION

Silicon nitride (Si_3N_4) balls for use in hybrid bearings have been shown to extend rolling contact fatigue (RCF) lifetime, reduce the dynamic loading in high-speed roller element applications because of their lower density (compared to historically used steel balls), and enable bearing use in more corrosive and higher temperature environments [1-3]. Many parameters such as density, hardness, elastic modulus, fracture toughness, 3- and 4-pt flexure strength and Weibull modulus, crushing strength, grain size and secondary phase morphology, porosity, and surface finish have been extensively studied in an effort to improve or predict RCF performance of Si_3N_4 balls [1-7]. As an outcome of many of those studies, ASTM F2094 [8] was developed and that specifies allowable minimums and maximums of many of those properties and finish conditions.

Surprisingly little or no study has been devoted to the quantification of sub-surface inhomogeneities (e.g., damage due to machining, residual effects from glass encapsulation used during hot-isostatic-pressing, etc.) and what effect they could have on RCF performance. Such sub-surface inhomogeneities usually play a dominant role in the performance (strength, fatigue,

¹ Research sponsored by the US Department of Energy, Office of FreedomCar and Vehicle Technologies, as part of the Heavy Vehicle Propulsion System Materials Program, under contract DE-AC-00OR22725 with UT-Battelle, LLC.

etc.) of structural ceramics. Its study in structural ceramics is typically facilitated using simple tensile or flexure strength specimen geometries that enable the concurrent measurement of strength and strength-limiting flaw size (latter identified through fractographical practices). However, for ceramic spheres, a likely historical barrier of their use to study strength-flaw-size relationships is the inherent geometry of the sphere itself; namely, it is nearly impossible to mechanically load a ceramic ball in a manner to produce a predictable tensile stress field at the sphere's surface sufficient to cause its fracture. Loading a ceramic sphere diametrically produces two Hertzian contacts, and ring- and cone-crack initiation can occur, and ultimate fracture can result if the contact stresses are sufficiently high. However, the evolution of ultimate fracture with this test makes the study of strength limitation from inherent flaws or other inhomogeneities located at the surface nearly impossible. Additionally, the fracture of brittle spheres from diametral compression occurs at such high loads (i.e., a great deal of stored energy exists in the sphere at fracture) that the test coupon disintegrates into fine rubble [9] rendering fractography nearly impossible, and thus, inhibiting the study of the relationship of strength-flaw size.

A new test coupon called the "C-sphere" flexure strength specimen was developed at Oak Ridge National Laboratory (ORNL) to enable the study of and measurement of a strength and linked flaw size. Enabling the identification of a flaw type (usually surface- or near-surface-located) and measurement of its size in finished ceramic balls is indeed important for the study of strength, but more importantly, for the study and predictability of RCF performance (a response limited by surface- or near-surface-located flaws or in changes thereof). Hadfield [10] reported that a critical depth of ring cracking in RCF is 5-20 microns below the surface; the C-sphere specimen is ideal for studying that near-surface depths.

The C-sphere specimen is produced through the controlled slotting of a ceramic sphere. It is then diametrically loaded (or flexed) to initiate fracture at the sphere's surface or "outer fiber". The C-sphere is analogous to a "C-ring" flexure specimen that is produced through the slotting of a ceramic ring. A description of the C-sphere flexure strength specimen follows and a comparison of the C-sphere flexure strength distributions of two commercially available Si_3N_4 bearing grade materials is presented.

C-SPHERE GEOMETRY

Initial Considerations

To work toward an optimized C-sphere geometry, a finite element analysis (FEA) model was created in ANSYS². The testing of the common ball diameter of 12.7 mm (0.50 in.) was the focus. Candidate slot widths of 3.175 mm (0.125 in.) and 6.35 mm (0.25 in.) were considered because they are common sizes for grinding wheel thicknesses, and the C-sphere machining would therefore likely be economical and have associated quick turn-around time. Slot depth was varied until a slot-width-slot-depth combination produced at least a 10-times higher outer-fiber surface tensile (hoop) stress than any other surface tensile stress located elsewhere on the coupon. The geometry of the final C-sphere is shown in Fig. 1. An offset between the original ball's center-line and the center-line of the 3.175 mm radius was deemed necessary because if the offset is zero or too small, then significant tensile stresses are created on the C-sphere's interior and a high likelihood that fracture would be initiated there because of both the high tensile stress and relatively rough surface finish produced by the grinding wheel. The final offset size (0.635 mm) resulted in a C-sphere geometry that, when diametrically compressed (see Fig. 2),

² ANSYS, Canonsburg, PA.

produced an outer-fiber tensile stress much larger than that on the ground interior and therefore a high likelihood that fracture would (desirably) occur there.

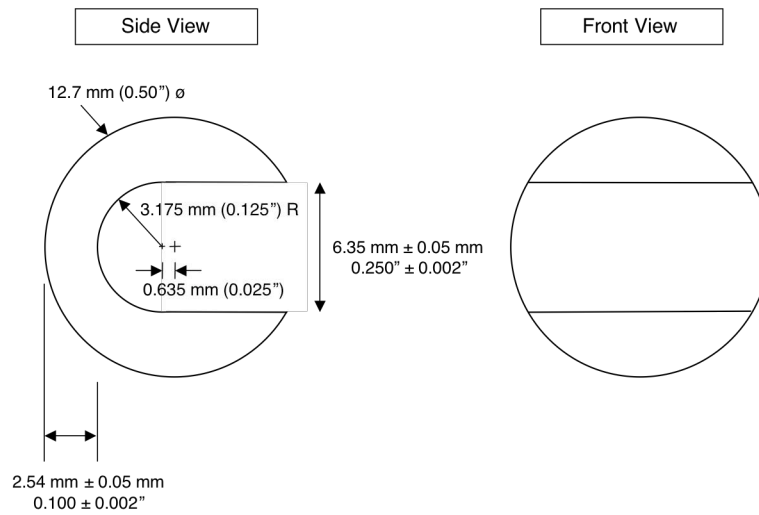


Figure 1. Side and front views of the C-sphere flexure strength specimen.

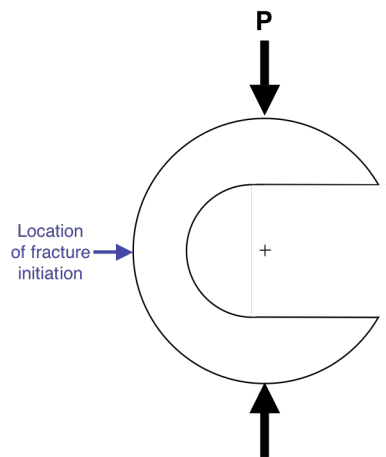


Figure 2. Diametral compression of the C-sphere flexure specimen causes fracture initiation from a hoop stress at the outer fiber.

C-Sphere Characteristics

A quarter symmetry model for the C-sphere flexure strength specimen was optimized and is shown in Fig. 3. Solid95 tetrahedral elements were used and a 100 N point load was applied to the C-sphere's apex. Several iterations of mesh density were evaluated. The resulting mesh contained 52703 elements and 76682 nodes, had fine mesh density in the region where high tensile stresses would develop, and gradually became coarser towards the area where the load was applied and in the overhang portion.

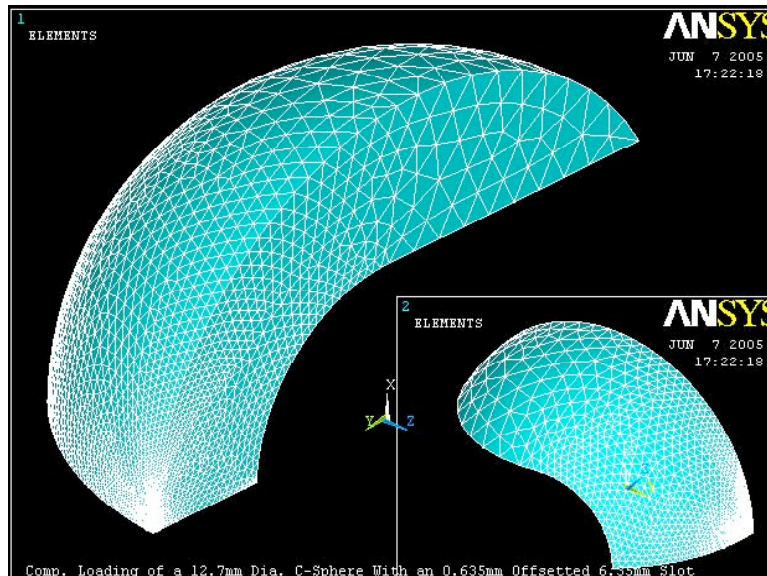


Figure 3. Mesh distribution for $\frac{1}{4}$ symmetry model of the C-sphere specimen, having 52703 elements and 76682 nodes.

The issue of artificially high stress concentration within the narrow zone under the applied point load and its effect on the computed effective sizes was considered. This is an idealization of what physically takes place where distributed load acting over a narrow area is actually applied. In other words, as the mesh gets finer the stress under the load will increase indefinitely making the model and hence the effective sizes mesh dependent. To understand the issue of stress singularity under the point load, both nodal and element 1st Principal stress distributions were studied. A nodal plot smoothes the stress distribution by averaging the stresses at that point in all the elements having that node in common. This smoothing is masking the very high stresses taking place within the individual elements, which if not removed would yield erroneous effective size calculations. This is because when the effective size is computed, the stress distribution is normalized with respect to the maximum effective stress in the component. If this maximum effective stress were incorrect, due for example to a localized stress concentration as is the case for this model, then the computed value would be incorrect. In order to unmask the high nodal stresses, element stress plots are used which display the actual nodal stresses as computed for each element.

In order to take out the effect of localized stress concentration on the effective size calculations, the artificially high stressed elements under the load point were removed. The

remaining elements, comprising the vast majority of the specimen, were then used to assess the specimen's effective area and effective volume. The nodal and element stress distribution plots for the C-sphere model, with the highly stressed elements carved out are shown in Fig. 4. One would then observe from these plots how the maximum tensile stress of 132 MPa shifts back to the side of the specimen where it should be. The fact that both the nodal and element stress plots yield the same stress distribution indicates that the suspect elements were successfully removed and that the remaining model can now be used to compute the effective sizes. Hence, it is the model shown in Fig. 4 that was utilized to compute the effective area and effective volume for the C-sphere specimen. Additionally, for Si₃N₄ C-spheres with the geometry shown in Fig. 1, the relationship between compressive load and outer-fiber maximum tensile stress can be determined from this model as well and is shown in Fig. 5.

Efforts are underway to validate predicted stresses from the model with experimentally produced stresses. For example, photo-stimulated luminescence spectroscopy (PSLS) was used with a compressively loaded alumina C-sphere to measure mean hydrostatic stress at the outer-fiber. The outer fiber tensile stress gradient is shown in Fig. 6 and compared to that predicted from the C-sphere FEA model. Predicted 1st Principal stress is expected to be higher than average hydrostatic stress for a given location, so this observed trend is not surprising. Comparison of predicted pressures is underway and that result will enable a fairer comparison of stress with experimental PSLS values. Additionally, a strain-gaged specimen is under preparation.

The effective area and effective volume as function of Weibull modulus for the C-sphere flexure strength specimen are shown in Fig. 7. The effective sizes were computed using the following equations [11]:

$$A_e = \left(\frac{\sigma_o}{\sigma_e} \right)^m \ln \left(\frac{1}{1 - P_f} \right) \quad (1)$$

$$V_e = \left(\frac{\sigma_o}{\sigma_e} \right)^m \ln \left(\frac{1}{1 - P_f} \right) \quad (2)$$

where A_e is the effective area, V_e is the effective volume, σ_0 is the scale parameter, m is the Weibull modulus, σ_e is the maximum effective stress (computed by CARES/Life³), and P_f is the probability of failure (also computed by CARES/Life). The effective sizes are independent of the scale parameter since they only vary with geometry, loading, and the Weibull modulus.

³ NASA Glenn Research Laboratory, Cleveland, OH.

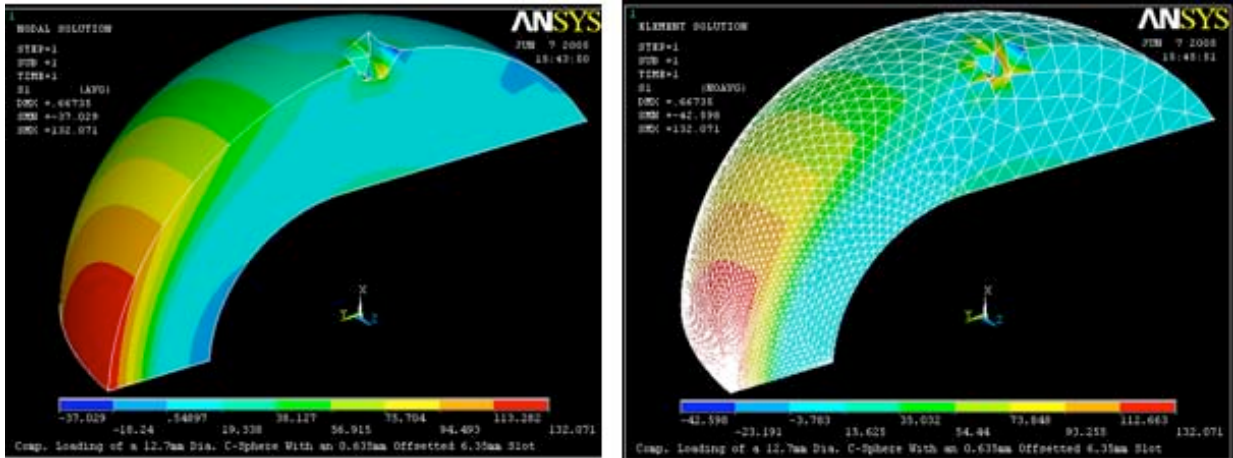


Figure 4. Nodal first principal stress distribution (left) and element 1st Principal stress distribution (right) for the C-sphere specimen with the elements within the high stress concentration zone (under the load) carved out.

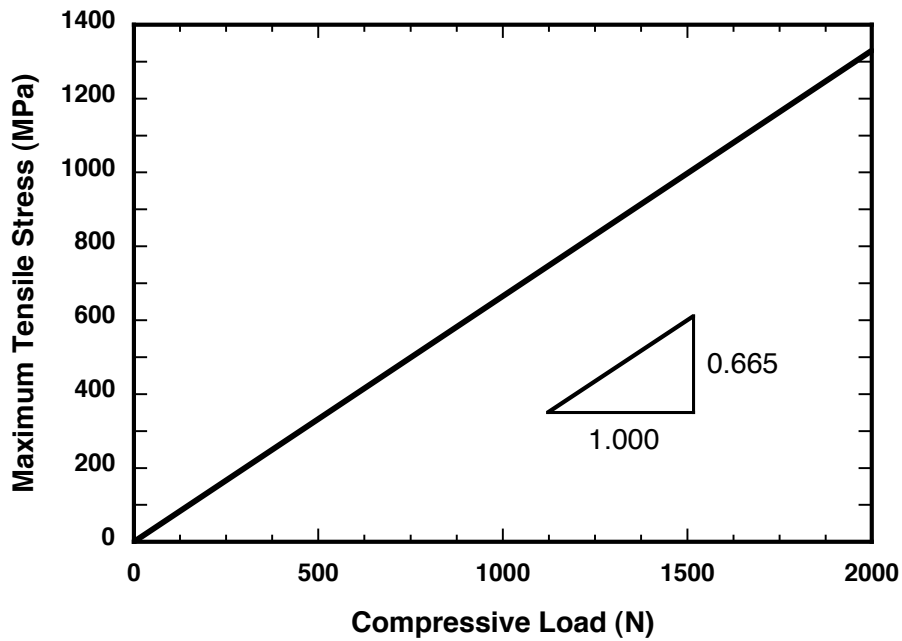


Figure 5. Maximum 1st Principal tensile stress (located at outer fiber - see Fig. 2) as a function of diametral compressive load for the C-sphere geometry in Fig. 1 for a Si₃N₄.

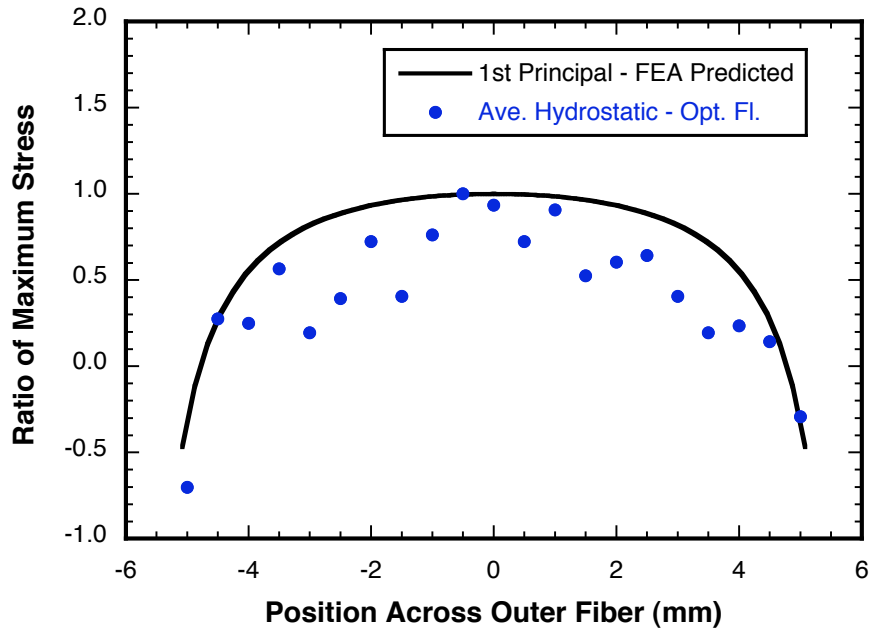


Figure 6. Comparison of predicted outer fiber stress and PLS-measured average hydrostatic stress. Predicted 1st Principal stress is expected to be higher than average hydrostatic stress for a given location, so this observed trend is not surprising.

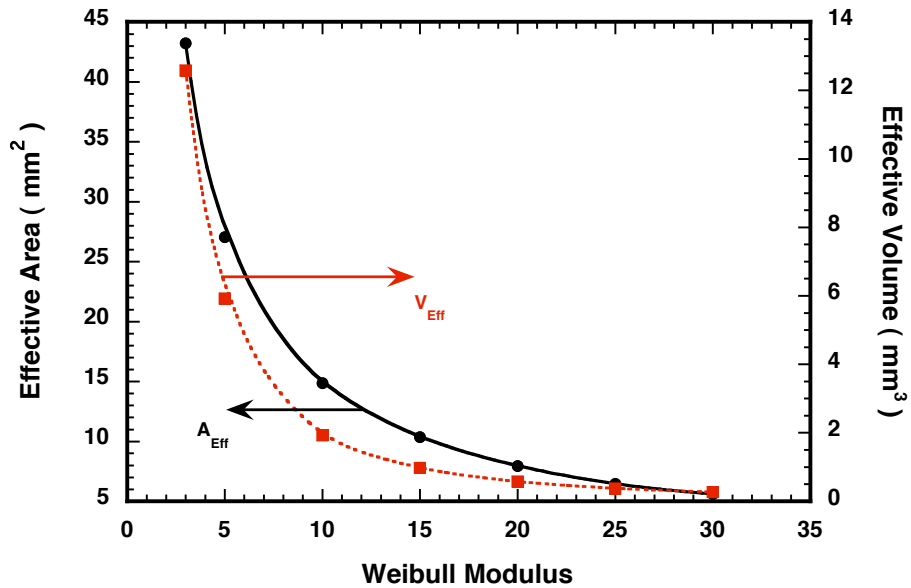


Figure 7. Effective area and effective volume as a function of Weibull modulus for the C-sphere flexure strength specimen.

C-SPHERE STRENGTH TESTING

NBD200 and SN101C balls with 12.7 mm diameter were machined⁴ into C-sphere flexure strength specimens (Fig. 8). Grinding of the slot was performed in a two step process using a Type 1F1 diamond plated grinding wheel (5 in. dia. x 0.25 in. thick with a full 0.125 in. radius or 127 mm dia. x 6.35 mm thick x 3.175 mm R) for the final grinding. Manufacturer⁵ reported properties for these two Si_3N_4 grades are shown in Table 1 and microstructural images of both are shown in Fig. 9. Elastic properties (needed in the FEA) of the two materials were measured with Resonant Ultrasound Spectroscopy [analysis method described in Ref. 12] and found to be close to the manufacturer's reported values (Fig. 10). The static and dynamic hardnesses of both materials were recently quantified [13].

C-sphere flexure specimens were monotonically and compressively loaded to failure using an electromechanical universal testing machine⁶ at a crosshead displacement rate of 0.5 mm/min. A special jig was used to horizontally align the C-sphere slot prior to loading. Load to fracture was recorded and used to determine C-sphere flexure strength according to Fig. 5. Weibull strength distributions were determined using commercially available software⁷. Optical fractography was conducted on all specimens to identify failure location and the fracture surfaces of a select few specimens were examined with scanning electron microscopy.



Figure 8. Si_3N_4 C-sphere flexure strength specimens.

⁴ Bomas Machine Specialties Inc., Somerville, MA.

⁵ Saint-Gobain Ceramics, East Granby, CT.

⁶ Instron Corp, Canton, MA.

⁷ WeibPar, Connecticut Reserve Technologies, Cleveland, OH.

Table I. Manufacturer reported information for the two tested Si_3N_4 materials [www.cerbec.com].

Property	NBD200	SN101C
Sintering Aid	MgO	$\text{Y}_2\text{O}_3 - \text{Al}_2\text{O}_3$
Density (g/cm^3)	3.16	3.21
RT Flexure Strength (MPa)	> 900	> 1000
Weibull Modulus	> 15	> 25
Elastic Modulus (GPa)	320	310
Poisson's Ratio	0.26	0.27
Vickers Hardness, HV10	1550	1600
Fracture Toughness ($\text{MPa}\sqrt{\text{m}}$)	> 5.5	> 6.5

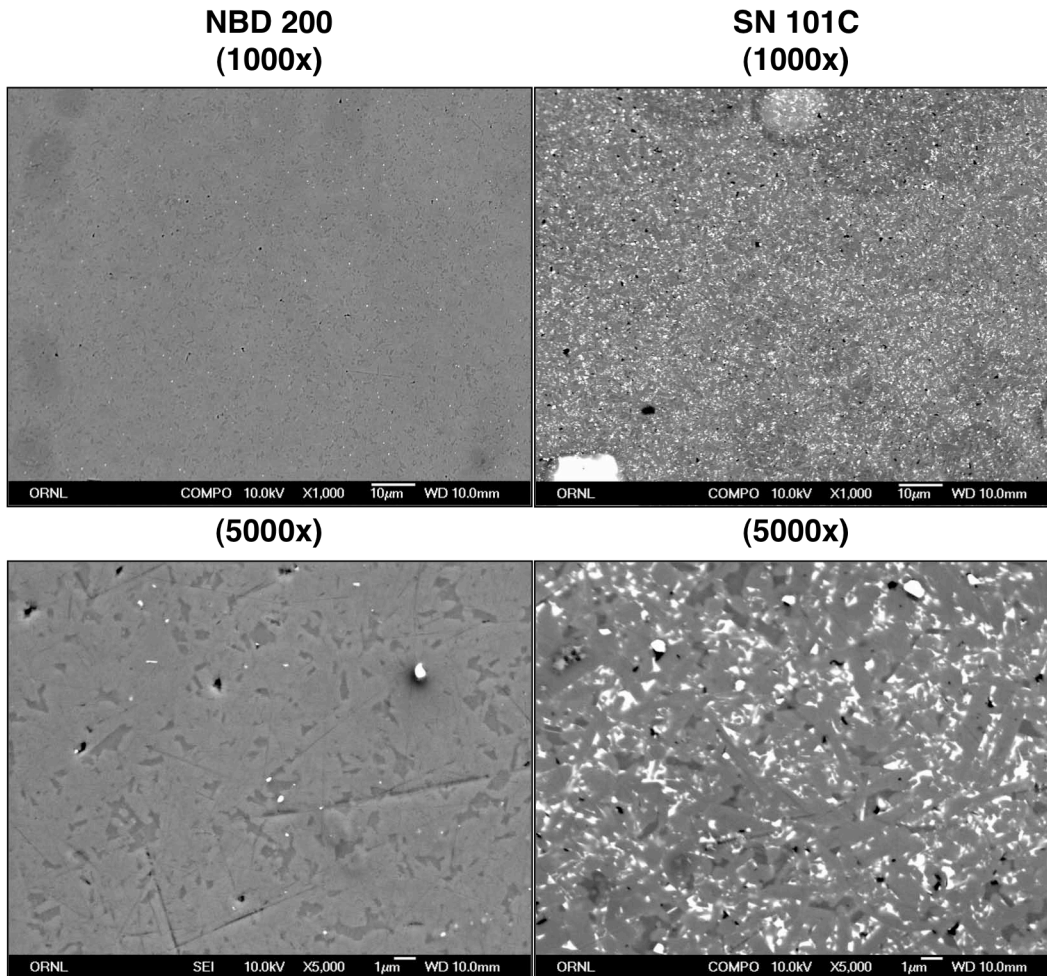


Figure 9. BS-SEM microstructure on finished ball surfaces of NBD200 and SN101C.

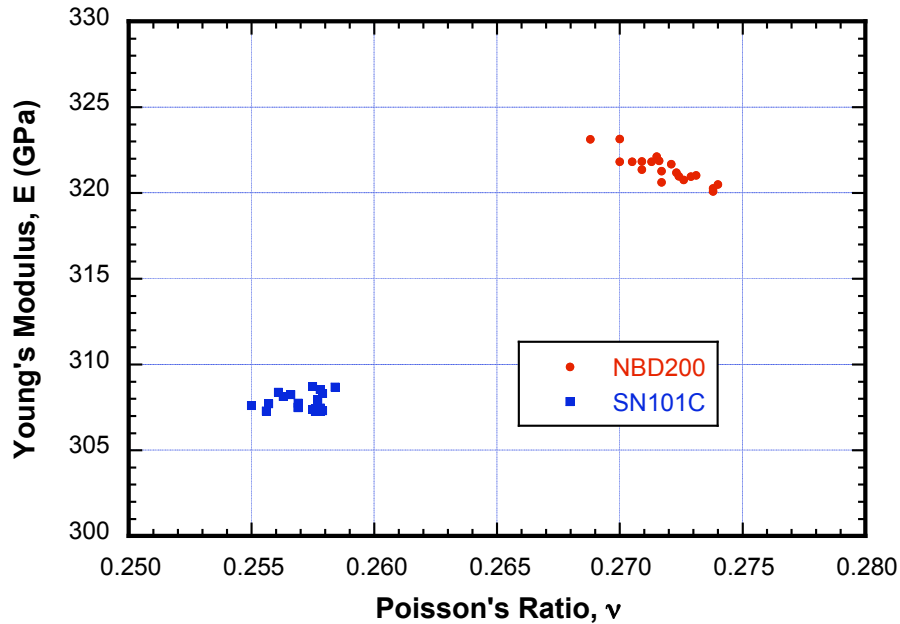


Figure 10. Elastic properties of NBD200 and SN101C measured using Resonance Ultrasound Spectroscopy.

RESULTS

The C-sphere characteristic strength of the SN101C was approximately 40% higher than that for the NBD200 (1081 MPa versus 778 MPa) while their Weibull moduli were statistically equivalent (6.0 and 6.5, respectively) - both those conclusions are made with 95% certainty. This difference in strength is illustrated in Figs. 11-12. Optical fractography showed that failure always initiated at the surface but not necessarily always exactly at the apex of the outer fiber (i.e., at zero position in Fig. 6). An example of one of those failure locations is shown in Fig. 13. According to the effective area dependence on Weibull modulus shown in Fig. 7, the effective area for a Weibull modulus of ~ 6 is approximately 20 mm^2 . As a comparison, the effective area for an ASTM C1161B bend bar [14] is approximately 100 mm^2 for a similar Weibull modulus. For a hypothetical situation where the same surface-type strength-limiting flaw is operative in both specimen geometries, the characteristic strength of that bend bar geometry should be $\sim 80\%$ of that for the C-sphere or $\sim 865 \text{ MPa}$ for the SN101C and $\sim 625 \text{ MPa}$ for the NBD200.

Work is ongoing as to how to interpret the meaning of C-sphere strength and fractography and how that may be related to potential RCF performance. For a strength of 770 MPa, a fracture toughness of $6 \text{ MPa}\sqrt{\text{m}}$, and a crack geometry factor of 1.5, the estimated Griffith flaw size for the specimen shown in Fig. 13 would be approximately 30 microns. That is of the size scale that Hadfield [10] had indicated to be a critical size for crack penetration during RCF. Many parameters have been studied and measured, and attempts have been made to link them to RCF performance. Could this C-sphere strength be a more useful and relevant parameter for Si_3N_4 ball manufacturers? C-sphere development work continues at ORNL.

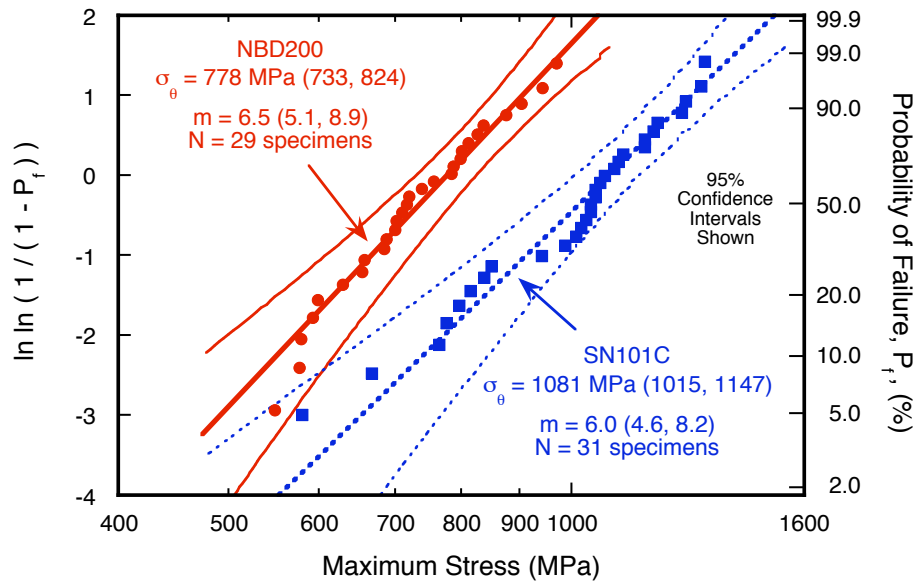


Figure 11. C-sphere Weibull strength distribution comparison of NBD200 and SN101C.

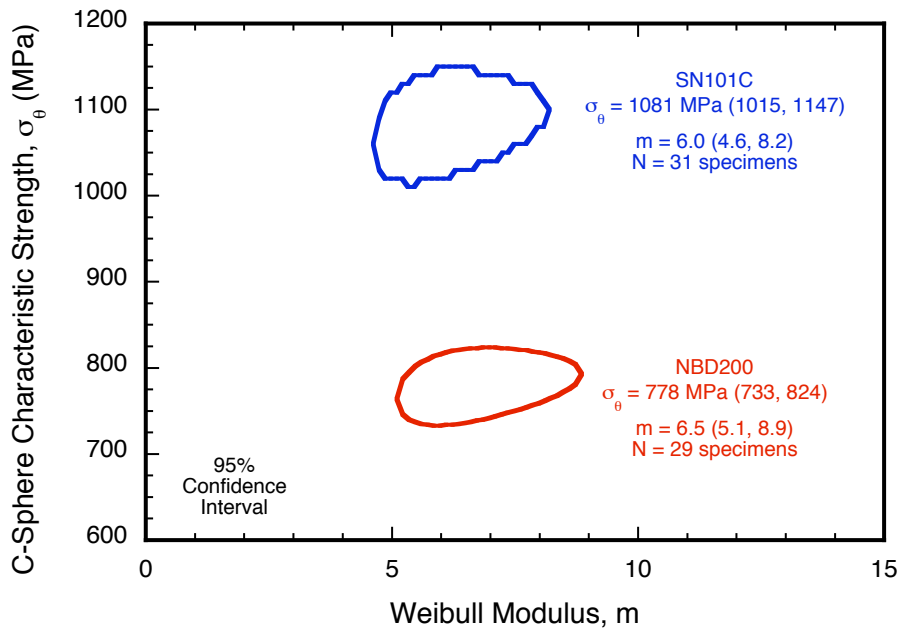


Figure 12. 95% confidence ratio rings for NBD200 and SN101C C-sphere strengths.

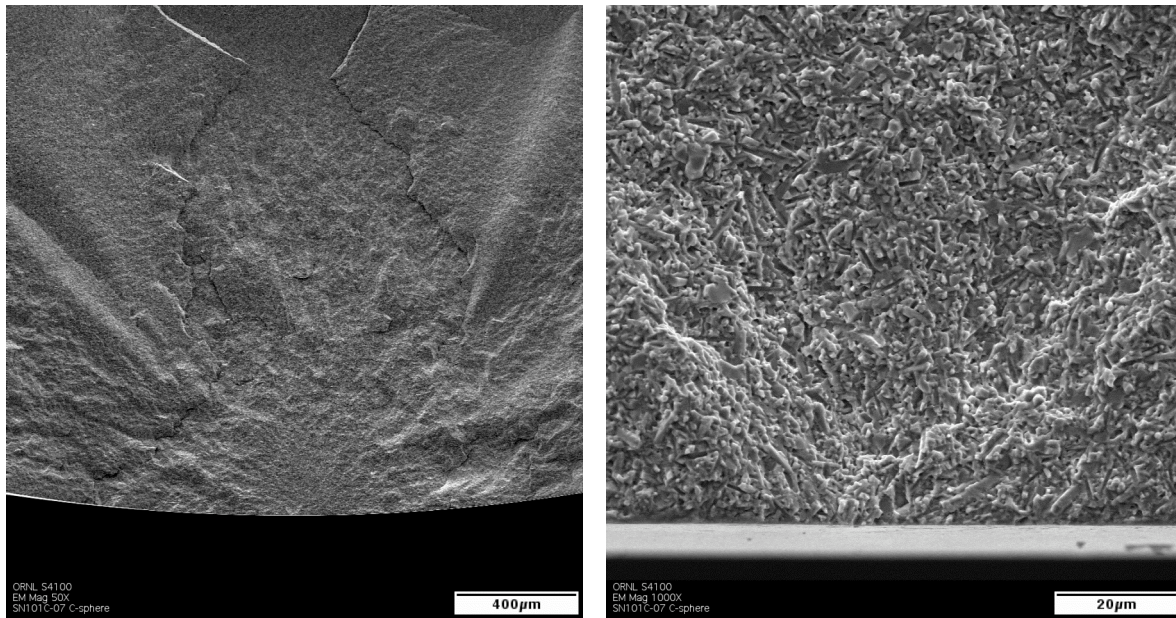


Figure 13. Example of a surface-located strength-limiting flaw in a SN101C C-sphere flexure strength specimen. This specimen had a strength of 770 MPa.

SUMMARY

A “C-Sphere” flexure strength specimen geometry was developed to effectively measure a relevant strength of bearing-grade Si_3N_4 balls and to relate that to the size-scale of surface-located strength-limiting flaws. C-sphere specimens are diametrically compressed to produce a monotonically increasing flexure or hoop tensile stress at their surface that cause their fracture. The strength is determined using the combination of failure load, C-sphere geometry, and FEA, and the stress field was used to determine C-sphere effective areas and effective volumes as a function of Weibull modulus. The SN101C bearing grade had a C-sphere characteristic strength approximately 40% higher than NBD200. Work is ongoing at ORNL to interpret the meaning of C-sphere strength and fractography and how that may be related to potential RCF performance and design of lower-cost Si_3N_4 ball bearing compositions with sustained RCF.

ACKNOWLEDGEMENTS

The authors wish to thank ORNL’s E. Kenik for the BS-SEM imaging, Bournemouth University’s M. Hadfield and Saint-Gobain’s V. Pujari for helpful discussions, and ORNL’s C. -H. Hsueh and J. Qu for their review of the manuscript.

REFERENCES

- [1] L. -Y. Chao and D. K. Shetty, J. H. Adair, J. J. Mecholsky, Jr., "Development of Silicon Nitride For Rolling-Contact Bearing Applications: A Review," *J. Mater. Educ.*, **17**, 245-303 (1995).
- [2] L. Wang, R. W. Snidle, L. Gu, "Rolling Contact Silicon Nitride Bearing Technology: A Review of Recent Research," *Wear*, **246**, 159-173 (2000).
- [3] Y. Wang and M. Hadfield, "Rolling Contact Fatigue of Ceramics," Vol. 11, Section 6E, ASM Handbook, 2002.
- [4] H. I. Burrier, Jr., "Optimizing the Structure and Properties of Silicon Nitride for Rolling Contact Bearing Performance," *Trib. Trans.*, **39**, 276-285 (1996).
- [5] J. Kang, M. Hadfield, and R. T. Cundill, "Rolling Contact Fatigue Performance of HIPed Si₃N₄ with Different Surface Roughness," *Ceram. Intl.*, **27**, 781-794 (2001).
- [6] M. Ichikawa, T. Takamatsu, T. Matsuo, N. Okabe, and Y. Abe, "Ring Crack Initiation Load of Silicon Nitride Bearing Balls," *JSME Intl. J. A: Mech. Mat. Engrg.*, **38**, 226-30 (1995).
- [7] R. T. Cundill, "Impact Resistance of Silicon Nitride Balls, pp. 556-61 in *Proc. 6th Intl. Symp. Ceram. Matls. Comp. Engines*, (1997).
- [8] "Standard Specification for Silicon Nitride Bearing Balls," ASTM F 2094-03a, Vol. 01.08, ASTM International, West Conshohocken, PA (2004).
- [9] B. A. Kschinka, S. Perrella, H. Nguyen, and R. C. Bradt, "Strengths of Glass Spheres in Compression," *J. Am. Cer. Soc.*, **69**, 467-72 (1986).
- [10] M. Hadfield, "Failure of Silicon Nitride Rolling Elements with Ring Crack Defects," *Ceram. Intl.*, **24**, 379-86 (1998).
- [11] J. B. Wachtman, *Mechanical Properties of Ceramics*, John Wiley & Sons, New York, 1996.
- [12] A. A. Wereszczak, "Elastic Property Determination of WC Spheres and Estimation of Compressive Loads and Impact Velocities That Initiate Their Yielding and Cracking," to be published in *Cer. Engrg. Sci. Proc.* (2006).
- [13] H. Wang and A. A. Wereszczak, "Mechanical Responses of Silicon Nitrides Under Dynamic Indentation," *Cer. Engrg. Sci. Proc.*, **26**, 275-283 (2005).
- [14] "Standard Test Method for Flexural Strength of Advanced Ceramics at Ambient Temperature," ASTM C 1161, Vol. 15.01, ASTM International, West Conshohocken, PA (2004).